Deep hole traps in boron-doped diamond

Pierre Muret,* Julien Pernot,† Amit Kumar, and Laurence Magaud
Institut Néel, CNRS and Université Joseph Fourier, 25 rue des Martyrs, BP 166, 38042 Grenoble Cedex 9, France

Christine Mer-Calfati and Philippe Bergonzo
CEA-LIST (Recherche Technologique), CEA-Saclay, 91191 Gif sur Yvette, France
(Received 5 February 2010; revised manuscript received 29 April 2010; published 4 June 2010)

Deep hole traps in boron-doped diamond epitaxial layers are studied by means of several types of deep-level transient spectroscopy and density-functional theory calculations. Standard deep-level transient spectroscopy and high-resolution isothermal transient spectroscopy permit to identify nine deep hole traps. Their capture cross-sections and ionization energies are systematically determined. In parallel, the ionization energies of donor and acceptor levels related to boron- and/or hydrogen-related complexes in diamond are assessed by *ab initio* calculations in this work and summarized with others from the literature including native defects. Tentative assignments of the measured deep hole traps to the calculated ones are proposed.

DOI: 10.1103/PhysRevB.81.235205 PACS number(s): 71.55.Cn, 73.20.Hb, 61.72.Bb

I. INTRODUCTION

Defects in semiconductors not only influence the electrical and optical properties of these materials but they also exhibit their own interesting physics. The identification and control of defects such as interstitials, vacancies, light atoms impurities like H or N in diamond, and their complex with host atoms is a major field of research, with important applications in materials engineering. Defects have been studied using a wide range of experimental techniques as electron paramagnetic resonance spectroscopy,[1,2] Hall conductivity,[3,4] positron annihilation,[5] and deep-level transient spectroscopy (DLTS).[6–8]

Diamond is still a very attractive material because of its exceptional physical and electronic properties.[9–11] In particular, diamond exhibits high carriers mobilities,[12–14] breakdown strength,[15] and thermal conductivity,[16] which enable diamond to surpass other wide band-gap materials for high-power and high-frequency electronic applications. However, the electronic properties of diamond are limited by defects and impurities introduced during the growth process and subsequent processing steps in the device fabrication. Therefore, improvement of the knowledge about this issue needs to understand and determine the electronic properties and lattice structures of defects and/or impurities in the diamond matrix.

Boron is known as the most effective acceptor impurity for diamond (with a ionization energy of $E_i \approx 0.38$ eV). A gradual change from semiconducting properties to metallic state and eventually to superconducting state is observed as the boron doping level increases from a few 10^{14} cm^{-3} above 5×10^{20} cm^{-3}.[17,18] However, it is pointed out that some boron atoms incorporated into diamond do not act as acceptors, and estimates relying on a combination of infrared-absorption spectroscopy and secondary-ion mass spectroscopy suggest that more than some tens percent of the impurities may be electrically inactive.[19] This might arise either if some boron atoms act as deeper acceptors or if they are passivated by some association with an other impurity like hydrogen or deuterium.[20–22] Alternatively, boron may segregate into highly defective regions of the material or within inclusions. Multiboron complexes, boron interstitials, and complexes of B with vacancies would be also candidate structures for defects resulting in a reduction in doping efficiency. There are experimental as well as theoretical calculations reports which suggest that heavily B-doped diamond contains nearest-neighbor-pair complexes which act as deep traps.[23,24]

Precise information about defects can be obtained by an analysis of the junction capacitance transients using DLTS. DLTS is considered as one of the most sensitive techniques to investigate the electronic behavior of deep traps in semiconductors.[25,26] Some authors have attempted to apply this kind of method to investigate shallow levels in either single crystalline or polycrystalline diamond[27–29] although not well adapted and have obtained mitigated results. On the contrary, deep hole traps with various activation energies and capture cross-sections have been reported experimentally in the last 20 years, first in polycrystalline diamond films,[30,31] then in single crystalline layers,[6,8,32–35] and from theoretical calculations.[23,24,36,37] But a complete understanding of their origin is still lacking. In the present work, we report the observation of deep hole traps in different homoepitaxial boron-doped diamond layers using electrical transient measurements. In Sec. II, the experimental details and *ab initio* method are described. In Sec. III, together with previously observed deep traps, a general insight is summarized and listed in Table I. In Sec. IV, density-functional theory (DFT) calculations of defect levels involving H and B are given and reviewed. Finally, in Sec. V and Tables II and III, we propose possible assignments of the observed DLTS deep traps to calculated donor or acceptor levels related to defects involving boron complexes and/or hydrogen.

II. EXPERIMENTAL AND CALCULATIONS DETAILS

A. Sample growth

Two boron-doped diamond films, called BM01 and BM02, were prepared on Ib (100) $3\times3\times0.5$ mm^3 Element Six substrates in the laboratory of the two last authors. Microwave-plasma-enhanced chemical vapor deposition was

TABLE I. Summary of the deep traps above the valence band studied by deep-level transient spectroscopy and high-resolution isothermal transient spectroscopy in boron-doped diamond films. BM01 and BM02 are the two samples investigated in this work. $[N_A-N_D]_{CV}$ is the net acceptor concentration measured by capacitance voltage technique. E_T-E_V is the free energy of the hole transition between the deep level and valence-band edge and σ the capture cross-section for holes, as defined in Eq. (1). N_T is the deep-level concentration in the samples.

Sample or Reference	$[N_A-N_D]_{CV}$ (cm^{-3})	E_T-E_V (eV)	N_T (cm^{-3})	σ (cm^2)	Traps label
32 and 35	7×10^{16}–9×10^{16}	1.57 ± 0.1	5×10^{14}–2×10^{16}	2×10^{-12}–8×10^{-12}	H_{1A}
BM02	1.9×10^{16}	1.57 ± 0.03	Not measured	1×10^{-11}–2×10^{-11}	H_{1B}
BM01	1.7×10^{17}	0.98 ± 0.04	Not measured	2×10^{-17}–6×10^{-17}	H_{1C}
BM01	1.9×10^{16}	1.08 ± 0.05	$\lesssim10^{16}$	6×10^{-16}	H_{1D}
BM02	1.7×10^{17}				
32 and 35	7×10^{16}–9×10^{16}	1.11 ± 0.04	10^{15}–10^{16}	1×10^{-18}–4×10^{-18}	H_{2A}
BM02	1.9×10^{16}	1.39 ± 0.03	2×10^{15} to $<10^{14}$	3×10^{-14}–9×10^{-14}	H_{3A}
BM02	1.9×10^{16}	1.26 ± 0.03	2×10^{15} to $<10^{14}$	1×10^{-15}–2.5×10^{-15}	H_{3B}
BM02	1.9×10^{16}	1.14 ± 0.07	10^{15} to $<10^{14}$	1×10^{-17}–9×10^{-17}	H_{3C}
BM02	1.9×10^{16}	1.24 ± 0.06	10^{15} to $<10^{14}$	1×10^{-17}–9×10^{-17}	H_{3D}
BM02	1.9×10^{16}	1.06 ± 0.09	10^{15} to $<10^{14}$	0.3×10^{-19}–11×10^{-19}	H_{3E}
BM02	1.9×10^{16}	0.78 ± 0.03	10^{15} to $<10^{14}$	1.2×10^{-22}–5×10^{-22}	H_{3F}
6	5×10^{16}–20×10^{16}	1.16 ± 0.03	Not measured	4×10^{-15}	
6	5×10^{16}–20×10^{16}	1.4 ± 0.07	Not measured	3×10^{-17}	
8	5×10^{16}	1.28	1×10^{16}	Not measured	
33	7×10^{15}	0.83	1×10^{15}	Not measured	
33	7×10^{15}	1.25	Not measured	Not measured	

carried out using methane (CH_4)-hydrogen (H_2) gas mixtures. The growth temperature, the pressure, the microwave power, and the ratio of CH_4/H_2, were fixed at 930 °C, 100 mbars, 600 W, and 0.3%, respectively. Boron incorporation was realized with trimethylboron residual in the reactor. The thickness of the two boron-doped layers were estimated to be 1.5 ± 0.1 μm. Lateral dot and plane (with ring-shaped-gap) Schottky barrier diodes[32,44] were fabricated on the boron-doped homoepitaxial diamond layer. Before fabrication of Schottky barrier diodes, the samples were cleaned in a mixture of sulfuric acid (H_2SO_4) and nitric acid (HNO_3) at 200 °C for 1 h to remove any graphitic layer and/or surface contaminations. Each Schottky contact pad (120-nm-thick Al film) was surrounded by the ohmic contact (30 nm Ti/40 nm Pt/50 nm Au) with 20 μm gap and there were nine Schottky contact pads in a 3×3 mm^2 size diamond sample. The diameter of each Schottky contact pad was 200 μm. The ohmic contact (Ti/Pt/Au) was annealed at 700 °C for 1 h in high vacuum (10^{-8} Torr) before fabricating the Schottky contacts. The gap between the Schottky diode periphery and the ohmic contact results in a series resistance and therefore a diode cut-off frequency for capacitance measurements $C(V)$ near 1 MHz between 300 and 400 K, depending of the sample. As the measurement frequency is also 1 MHz, the boron doping concentrations are deduced from $C(V)$ at 600 K for ensuring that the cut-off frequency of the diodes are well above the measurement frequency. They amount in average to 1.7×10^{17} cm^{-3} and 1.9×10^{16} cm^{-3}, respectively, in samples BM01 and BM02.

B. Deep-level transient spectroscopies

DLTS is a high-frequency capacitance transient method useful for observing a wide variety of deep centers in semiconductor junctions like Schottky diodes, where the depletion zone width can be controlled by the applied voltage. The electrical transients due to majority carrier emission take place under reverse-bias voltage after an electrical pulse at a lower or zero-reverse-bias voltage, which shrinks the depletion zone width and fills the deep levels momentarily included in a slice of the neutral zone with majority carriers, here holes. When the reverse-bias voltage is restored, a multiphonon-assisted transition drives the population of majority carriers trapped on the deep level toward its previous equilibrium value inside the same slice which is now incorporated again into the depletion zone. If only one deep level is involved, this population follows the exponential decreasing law characterized by a time constant which is, in fact, the inverse of the transition probability per unit time W, commonly called the emission rate e_p, in a p-type semiconductor. It can be monitored either from the transient current or charge, or capacitance, or voltage if the capacitance of the junction is maintained constant by a feedback loop in the last case. In this work, the capacitance-voltage (C-V) and capacitance transient $\Delta C(t)$ measurements are performed in a broad temperature range, able to scan the 85–870 K interval, using a Phystech FT 1030 digitizing DLTS system,[45] a Linkam temperature controller and sample holder, and some additional algorithms which are detailed further. At the measurement frequency of 1 MHz, the capacitance of the reverse-biased junction follows linearly the deep-level population if

TABLE II. Summary of the deep donor levels related to boron, hydrogen, or native defects in the diamond band gap calculated by *ab initio* method and tentative attribution to traps observed by deep-level transient spectroscopy. Deep levels deduced from DLTS and donor level *ab initio* calculations summarized in this table are extracted both from this work and references of the literature.

Donor level	Energy level (eV)	Reference	Possible DLTS traps
H	$E_c-3.26$	This work	No
	$E_c-3.0$	38	No
	$E_c-2.8$	39	No
	$E_c-3.0$	40	No
H_2	$E_c-4.84$	This work	H_{3F}
	Close E_v	38	H_{3F}
B_2	$E_c-4.9$	This work	H_{3F}
B_i	$E_v+4.8$ to 2.4	41	No
I	$E_v+2.5$	41	No
B_SI	$E_v+2.2$	41	No
BH	$E_c-4.84$	42	H_{3F}
BH_2	$E_c-2.8$	42	No
	$E_v+2.6$ or 2.9	41	No
	$E_c-1.84$ to 2.88	40	No
BH_3	$E_v+0.2$	41	No
BH_4	$E_v+1.8$	41	No
V	$E_v+0.6$	43	H_{3F}
B_SV	$E_v+1.0$	24 and 41	H_{1C}, H_{2A}, H_{3i}
B_SVH	Close E_v	41	H_{1C}, H_{2A}, H_{3i}
B_SVH_2	Close E_v	41	H_{1C}, H_{2A}, H_{3i}
B_SVH_4	Deep	41	No

TABLE III. Summary of the deep acceptor levels related to boron, hydrogen, or native defects in the diamond band gap calculated by *ab initio* method and tentative attribution to traps observed by deep-level transient spectroscopy. Deep levels deduced from DLTS and acceptor level *ab initio* calculations summarized in this table are extracted both from this work and references of the literature.

Acceptor level	Energy level (eV)	Reference	Possible DLTS traps
H	$E_v+3.07$	This work	No
	$E_c-1.8$	38	No
	$E_c-1.45$	40	No
H_2	$E_v+4.69$	This work	No
B_S	$E_v+0.2$	24	No
B_2	$E_v+1.0$ to 1.2 (-,0)	24	H_{1A}, H_{1B}, H_{3A}
	$E_v+2.5$ to 2.6 (--,-)	24	No
	$E_v+1.214$	This work	H_{1A}, H_{1B}, H_{3A}
B_i	$E_c-0.1$ to 1.1	24	No
I	$E_c-1.9$	41	No
B_SI	$E_c-1.8$	24 and 41	No
B_SB_i	Deep	24	No
BH	$E_c-1.00$	40	No
	$E_v+4.44$	42	No
BH_2	$E_v+1.14$	42	H_{1A}, H_{1B}, H_{3A}
	$E_v+1.6$ to 1.9	41	H_{1A}, H_{1B}, H_{3A}
B_2H	$E_v+0.2$	23	No
V	$E_c-2.5$	43	No
V_2	$E_v+1.7$	43	H_{1A}, H_{1B}, H_{3A}
B_SV	$E_c-3.6$	24 and 41	H_{1A}, H_{1B}, H_{3A}
B_2V	$E_c-3.9$	24	H_{1A}, H_{1B}, H_{3A}
B_3V	$E_c-5.6$	24	No
B_4V	$E_c-5.6$	24	No
B_SVH	Midgap	41	No
B_SVH_2	Midgap	41	No
B_SVH_3	$E_c-2.5$	41	No
B_SVH_4	Deep	41	No

the deep-level concentration stays below some tens percents of the shallow concentration, a case which is achieved in the samples under study. After a filling pulse of duration t_p, transients are repetitively recorded during the time window t_w so that an averaged digitized signal is obtained in each time window. Different ways may be used for processing this signal and plotting the result. Here, Fourier transform DLTS (Ref. 46) is preferred because it opens the route for a quantitative analysis of the response and appears as the more natural method for extracting the emission rate since the spectrum derived in this way lies in the frequency domain, of same dimension as the emission rate. Indeed, for a single exponential transient lasting t_w, each Fourier coefficient of rank n of the transients, either the real a_n or the imaginary part b_n, contains quantitative information about this emission rate e_p, which can be extracted from the maximum position in the spectrum, plotted as a function of the frequency when isothermal transient spectroscopy (ITS) is used. The frequency is simply obtained from n/t_w. Alternatively, DLTS relies on the emission-rate changes induced by temperature, which yields again a bell-shape curve when recorded at constant frequency. In the two methods, the spectra involve unique relationships both between (i) the maximum position against the emission rate at each temperature and (ii) the amplitude of the peak against the deep-level concentration N_T. This later quantity is evaluated in this work using this method. From the detailed balance principle, the emission rate or equivalently the transition probability per unit time can be expressed under the following form:[25,26]

$$\frac{e_p}{T^2} = \frac{W}{T^2} = \gamma\sigma \exp\left[-\frac{(E_T - E_V)}{kT}\right], \tag{1}$$

where E_T-E_V is the free energy of the transition, σ the capture cross-section for holes, which may be thermally activated, and γ is a material constant defined as,

$$\gamma = (96\pi^3)^{1/2} g \frac{m^* k^2}{h^3}, \tag{2}$$

where m^* is the hole effective mass, h is Plank's constant, and g is the degeneracy factor. The γ value for holes in

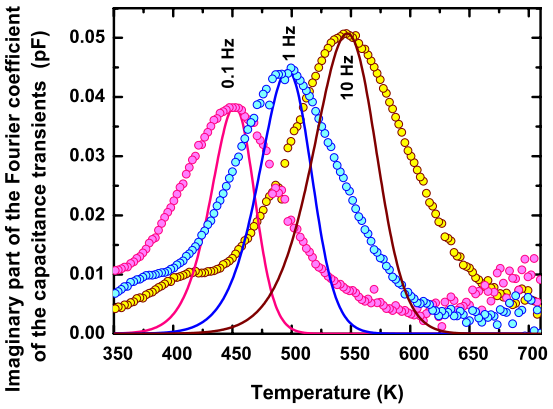

FIG. 1. (Color online) Experimental deep-level transient spectra featured as the imaginary part of the first-order Fourier coefficient of the transients for three frequencies (circles) and simulated spectra (full lines) whose maximum position is adjusted to match the experimental curve with the help of only one capture cross-section, in one diode made on the sample BM01. Simulated curves are calculated with a free energy of ionization of 0.98 eV and a capture cross-section of 3.2×10^{-17} cm^2.

diamond is 2.6×10^{21} cm^{-2} s^{-1} K^{-2} if $g=1$. The slope of the Arrhenius plot e_p/T^2 versus $(1000/T)$ yields the activation energy, which is the free energy of the transition only if the energy barrier for capture can be neglected. However, this latter quantity is generally considered as included in the uncertainty coming from the random deviation of data to a straight line. Then, as shown in Fig. 1, simulated spectra can be plotted and the position of their maximum is adjusted to experimental data with the help of a single capture cross-section, which is therefore obtained at the temperature where the maximum of the spectrum takes place. In this way, the capture cross-section is derived with a fairly good accuracy because it depends only on the activation energy uncertainty, as deduced from that happening on the slope of the Arrhenius diagram. Moreover, it is determined at the actual temperature, without the large inaccuracy which characterized the old method relying on the intercept of the vertical axis in the Arrhenius diagram, at infinite temperature. Such an improvement is very useful for getting the charge state of the defect before capture of a carrier with a much higher degree of truth than in the past. However, as shown in Fig. 1, the simulated spectra, which are based on a Dirac-type distribution of the emission rates, meaning that only one emission rate plays a significant role at each temperature, is narrower than the experimental one. Such a result is almost systematically encountered in diamond and indicates a more complex distribution function $g(W)$ for the emission rates. This is the reason why Fourier transform DLTS and specially high-resolution isothermal methods are preferred here. These more relevant tools for approaching a realistic distribution function $g(W)$ consist in high-resolution ITS (HR-ITS), either based on a Tikhonov regularization analysis of the transients recorded along a logarithmic time scale[6,32,47] or the same algorithm both applied to imaginary and real parts of the Fourier transform of the transients.[48] These methods will be used when complex distributions of emission rates happen.

C. *Ab initio* calculations

The structure and electronic properties of isolated hydrogen, hydrogen-hydrogen, boron-boron, and boron-hydrogen complexes were investigated using the Vienna *ab initio* simulation package (VASP) code.[49] It is based on DFT within the generalized gradient approximation.[50] Projector augmented wave is used with a basis cutoff equal to 318.6 eV.[51] The Monkhorst-Pack scheme[52] with $5\times5\times5$ k points has been used for integration in the Brillouin zone. The error of total-energy convergence is smaller than 10^{-4} eV. The densities of states are calculated using the tetrahedron method with Bloechl corrections. The calculation of the energy band gap for pure diamond ($E_g=4.2$ eV) is in good agreement with theoretical calculations.[40,53]

Non-neutral charged states were modeled by adding or subtracting one electron to the system. A uniform background is then automatically added by VASP to keep a neutral system and avoid problems related to coulomb energy of ordered interacting charged defects. The error associated to this procedure is reduced for large cells such as the $3\times3\times3$ to $4\times4\times4$ cubic cell.

Calculation of ionization energies is not straightforward because of the well-known drawbacks of the DFT approach: it does not lead to a good value of the gap width[54] and the Kohn Sham levels—eigenvalues obtained by the *ab initio* calculation—have no clear physical meaning and should not be used as the quasiparticle energies. Furthermore, there is no absolute energy reference in *ab initio* calculations that involve different atomic concentration so no way to fix the conduction-band minimum. As we are dealing with point defects, the geometry and then the related electronic level of the defect can change with its state of charge. So that the most stable configuration have to be searched for each charge state to evaluate the ionization energy. There are several methods for calculating the electrical energy levels of defects, none of them has become universally accepted. The formation-energy method involves comparison of the calculated formation energies of defects in different charge states.[55] Recently, marker method has been successfully used for electrical energy-level calculations, in the case of boron-hydrogen complex in diamond, chalcogen defects in diamond and silicon.[40,41,53,56–58] This method eliminates some of the errors in DFT calculations, such as an underestimation of the band gap, which may influence the position of the defect levels and systematic errors coming from the compensating background for charged defects.[56,59] In present study, the marker method is employed to investigate ionization energies. It scales the searched ionization energy using another known defect—the marker—for which this value is well known as described in Ref. 42.

III. EXPERIMENTAL RESULTS AND ANALYSIS

A. Fourier transform deep-level and isothermal transient spectroscopies

Fourier transform DLTS spectra, consisting here in the first-order imaginary Fourier coefficient of transients measured at three frequencies as a function of temperature in

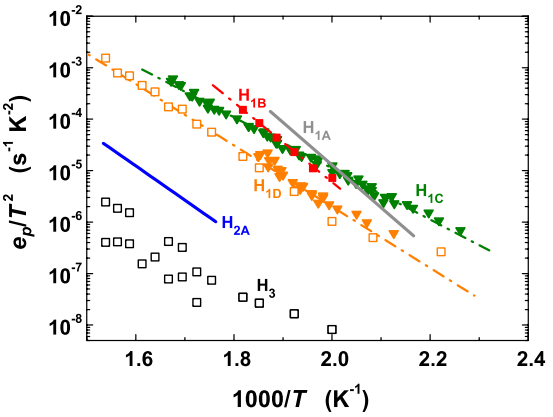

FIG. 2. (Color online) Arrhenius diagram of deep hole traps, i.e., the hole emission rate divided by the square of the temperature (e_p/T^2) against 1000/T as defined in Eq. (1), in boron-doped diamond layers. Symbols have been obtained in this study in samples BM01 (triangles) and BM02 (squares), while full lines feature results already published in the literature (Refs. 32 and 35). The full symbols aligned along dashed-dotted lines are deduced from the classical method described in the text, while open symbols come from the high-resolution isothermal transient spectroscopy method. The physical parameters of the deep traps labeled in this figure are summarized in Table I.

sample BM01, are shown in Fig. 1. All the Fourier coefficients a_n and b_n and various correlation functions like those using square wave kernels[46] display similar bell-shape curves, with a characteristic ratio between the emission rate and the frequency for each of them at their maximum if a single emission rate is assumed to operate at each temperature. Therefore, emission rates can be derived for all the temperatures where some coefficient passes through a maximum value and then plotted in an Arrhenius diagram like shown in Fig. 2, which allows to deduce the activation energies. Then, the capture cross-section is adjusted in order that the maximum of each simulated Fourier coefficient or correlation function matches the experimental one, like in Fig. 1. The couple of these two parameters, namely, the activation energy and capture cross-section, is the signature of each deep level and appears as a straight line located at a unique place in the Arrhenius graph. The results are summarized in Table I and Fig. 2, where results derived with the help of the method described before appears with full symbols aligned along dashed-dotted lines. Already published results[32,35] are displayed in full lines without data points while open symbols come from the HR-ITS method detailed in the following.

B. Analysis of transients recorded along a logarithmic time scale

As pointed out previously in this paper and former references, the DLTS spectra are generally not well fitted by the theoretical law calculated from the Fourier transform of a single exponential transient with a single emission rate at each temperature, which reads $\exp(-e_p t)$ or $\exp(-Wt)$, where t is the running time. Consequently, it is advisable to consider that the transients and their Fourier spectra result from a multiple transient law which can be written $\Delta C(t) = \int_0^\infty g(W)\exp(-Wt)dW$, taking the emission-rate distribution $g(W)$ into account. This expression looks like Laplace transform[60,61] but differs in several respects. First, it should be rather an inverse Laplace transform since the integral is calculated in the emission-rate domain, not in the time domain. Second, the variable W is a real quantity, as expected for an observable, not a complex one. Third and more importantly, the left-hand side is known from measurements, with an unavoidable superimposed noise, whereas the distribution $g(W)$ has to be determined in the right-hand side of the equation, which is a Fredholm integral. This calculation requires the inversion of this Fredholm integral equation and, therefore, to solve an ill-posed problem. Nevertheless, a reliable estimate of the distribution function can be derived with a regularization method.[47,62,63] The FTIKREG algorithm from Weese[63] with the $\exp(-Wt)$ kernel is used here because it has proven its robustness along many trials that we have performed to extract reliable distribution functions from experimental transients in large gap semiconductor junctions. In addition to the sum of all the squares of the difference between the experimental data and the right-hand side of the Fredholm equation, taken from every measurement and normalized by the experimental uncertainty, a third term, motivated by the theory of Tikhonov regularization, prevents the experimental errors from having too a large influence on the result. This third term is chosen proportional to the norm of the distribution function $g(W)$ and is weighted by the so-called regularization parameter which has essentially the same meaning as the bandwidth of a filter for smoothing noisy data. In the minimization procedure, an optimal value of the regularization parameter is calculated in FTIKREG, but can also be given by the user in order to check its influence on the result. As indicated by the author[63] and easily checked by applying the algorithm to any simulated transient, the exact solution for $g(W)$ is indeed obtained if no noise is added to the transient data calculated from an arbitrary distribution function $g(W)$. The main effects of the superimposed noise included into the real measured data consist in a broadening and eventually slight shifts of the structures of $g(W)$, as we have checked from simulated data. Moreover, the expression $\Delta C(t) = \int_{\ln W_{min}}^{\ln W_{max}} g(\ln W)\exp(-Wt)d(\ln W)$ is preferred because all the quantities experience very large variations in the frequency and in the time domain as well. Similarly, the transients, initially recorded as a function of a linear time scale for many time windows, ranging from some hundreds microsecond to thousand seconds, are joined together in order to build a logarithmic transient at each temperature, which displays the capacitance variation as a function of the logarithm of time, like shown in Fig. 3.

Applying the FTIKERG algorithm to the data of Fig. 3 allows to deduce the experimental distribution functions $g(W)$ displayed in Fig. 4. One can see that two groups of structures emerge: (i) at highest emission rates, a broad peak, its full width at half maximum being close to one decade, associated to a tail comprising generally several overlapping peaks on its lower abscissa side; (ii) continuing toward the lowest emission rates, two peaks can be distinguished, at

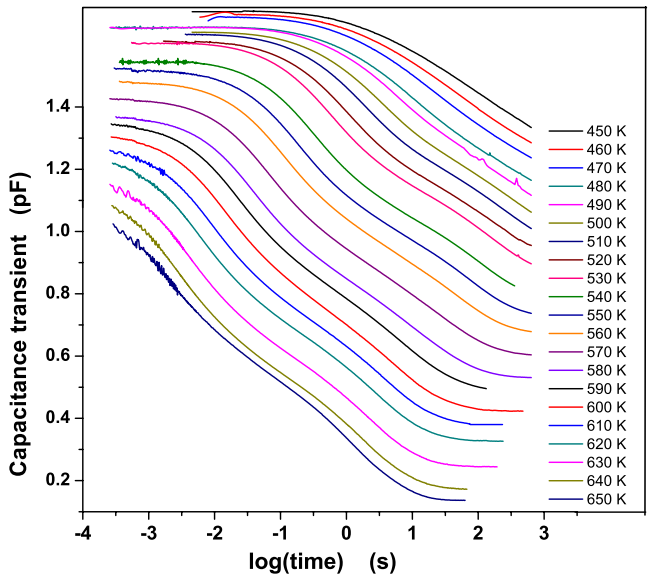

FIG. 3. (Color online) Capacitance transients plotted as a function of the logarithm of time for several temperatures in one diode of the boron-doped diamond sample BM02. The reverse-bias voltage is 1 V. The filling pulse lasts 0.5 s and its voltage level amounts to −1.5 V in forward bias. As a consequence, deep levels are probed in a slice comprised approximately between 90 and 150 nm below the Schottky contact.

least between 650 and 580 K, while dispersion of the distribution increases at the lowest temperatures. The shape of $g(W)$ is generally stationary along the different temperatures, apart from the expected shift of the peaks toward lower emission rates when the temperature decreases. However, the superimposed noise being not the same from one measurement to the subsequent one, the width of the peaks in a distribution may experience large variations in few cases in Fig. 4. Such

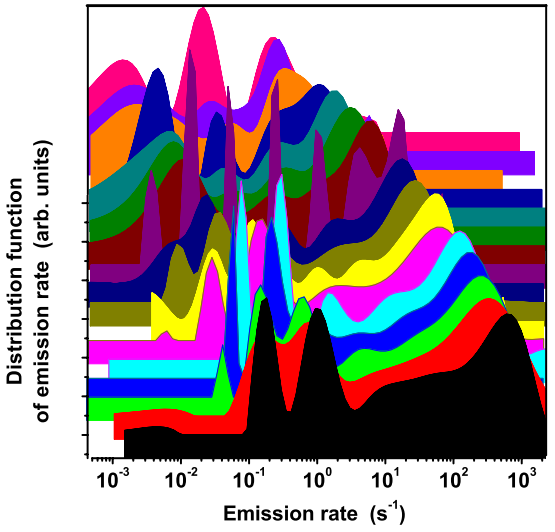

FIG. 4. (Color online) Distribution function $g(W)$ of the emission rates for temperatures decreasing from 650 K at the bottom of the figure to 490 K at the top, with 10 K steps, deduced from applying the FTIKREG algorithm to transients of Fig. 3 for boron-doped diamond (sample BM02).

a drawback can be largely corrected with the next method. The large dispersion of the emission rates at each temperature indicates unambiguously that deep levels are multiple and each of them has either ionization energy or capture cross-section, or both, which undergoes some variation, detected with a much higher resolution than in the standard ITS or DLTS methods. Such a broad distribution is not expected for point defects, except under uniaxial pressure to a limited extent[61] or some other external perturbation which is not present here. Consequently, it is likely that the deep levels detected in these samples are related to complex and extended defects, in which variability of the site environment and inhomogeneous internal strain and electric field may induce a significant dispersion of the physical characteristics of the levels.

C. Direct analysis of isothermal spectra in the frequency domain

As many transients of increasing duration t_w are recorded, their Fourier transforms are simultaneously calculated for frequencies n/t_w, n being an integer. The imaginary and the real parts of the Fourier transform of the transients shown in Fig. 3 are displayed in Fig. 5 with $n=1$. Since the quantities which are searched at each temperature consist in emission rates, it is more natural and efficient to deal with data that are already in the frequency domain, where they appear as a set of peaks. The FTIKREG algorithm can also be applied to a double set of data, which are the images of dispersive and dissipative parts of a physical quantity like in Ref. 48. Here, taking into account the recording of the experimental transient with a delay settled to $t_0=t_w/4$ after the end of the filling pulse, the two Lorenzian kernels corresponding to the imaginary $B_n(f)$ and the real $A_n(f)$ parts of the Fourier transform of the retarded transient $\exp[-W(t+t_0)]$, with the fundamental frequency $f=1/t_w$, read

$$B_n(f) = \pi n \exp[-W/4f]\frac{1-\exp(-W/f)}{(W/f)^2+(2\pi n)^2}, \tag{3}$$

$$A_n(f) = \frac{W}{2f}\exp[-W/4f]\frac{1-\exp(-W/f)}{(W/f)^2+(2\pi n)^2}. \tag{4}$$

The FTIKREG algorithm is now used with these two kernels to derive the most probable distribution of emission rate from the imaginary and the real parts of the simulated spectrum, respectively, $\int_{\ln W_{min}}^{\ln W_{max}} g(\ln W)B_n(f)d(\ln W)$ and $\int_{\ln W_{min}}^{\ln W_{max}} g(\ln W)A_n(f)d(\ln W)$ because Fourier transform is a linear operator. These quantities are compared in the same way as in the previous time-domain method to the experimental data displayed in Fig. 5 at each temperature. The whole information contained in experimental data is basically the same as before Fourier transformation, but now it is dispatched along the frequency axis, of same dimension as the emission rate and the constraint of matching the same distribution $g(\ln W)$ for both the imaginary and the real parts of the spectrum independently, is more stringent. Moreover, the superimposed noise appears as a smoother contribution than in the time domain where it is a random additive com-

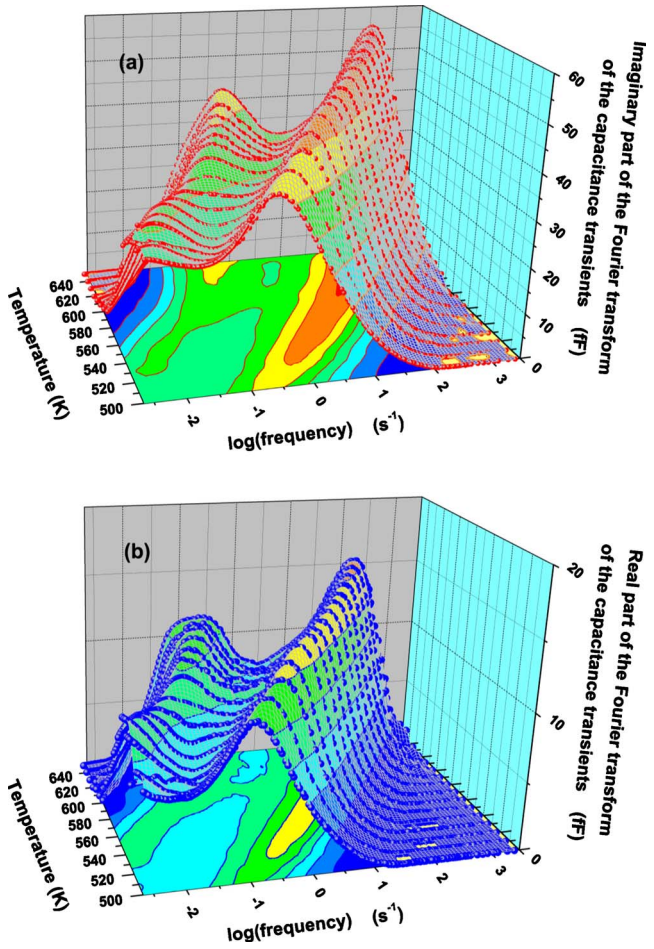

FIG. 5. (Color online) Set of isothermal spectra or equivalently, (a) the imaginary and (b) the real parts of the Fourier transform of the capacitance transients shown in Fig. 3 from 650 to 500 K by 10 K steps, as a function of the fundamental frequency, for boron-doped diamond (sample BM02).

ponent. Its effect can be partially controlled by adjusting the relative amplitude of the two parts of each isothermal spectrum in order that the width of the peaks of $g(\ln W)$ reaches its minimal value and remains more or less constant throughout the whole temperature range, as displayed in Fig. 6. However, the ultimate effect of noise consists in broadening the peaked structures of $g(\ln W)$ and it cannot be removed. Here also, the exact distribution function would be obtained if no noise were present. Then, the question of the real width of the structures contained in the distribution function is raised. As shown in Fig. 7, both the imaginary and the real simulated spectra calculated with the help of the quasicontinuous distribution function displayed at 580 K in Fig. 6 perfectly match the experimental spectra whereas a multipeaked distribution comprising only the Dirac-type components pertaining to the maxima of Fig. 6 at 580 K leads to an oscillatory behavior which does not exist in the experimental spectra. This is a first indication of the quasicontinuous nature of the distribution function of the emission rates. In other words, a physical reason causes a broadening of the emission-rate structures which cannot be entirely ascribed to the mathematical processing. An other benefit of this method

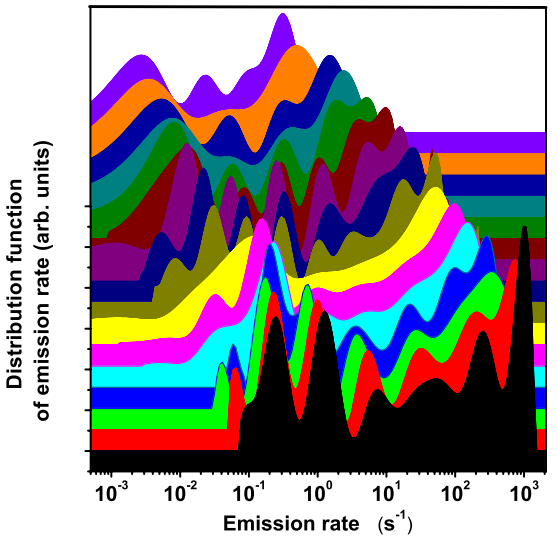

FIG. 6. (Color online) Distribution function $g(\ln W)$ of the emission rates for temperatures decreasing from 650 K at the bottom of the figure to 500 K at the top, with 10 K steps, deduced from applying the FTIKERG algorithm to the imaginary and the real isothermal spectra in Fig. 5 for boron-doped diamond (sample BM02).

comes from the prefiltering operated by the Fourier transformation, which finally increases the resolution, as it can be seen in most spectra of Fig. 6 in comparison to Fig. 4. From all these considerations, it turns out that the frequency domain processing method is more robust and reliable, give distribution functions with higher resolution and for these reasons deserves to be named HR-ITS.

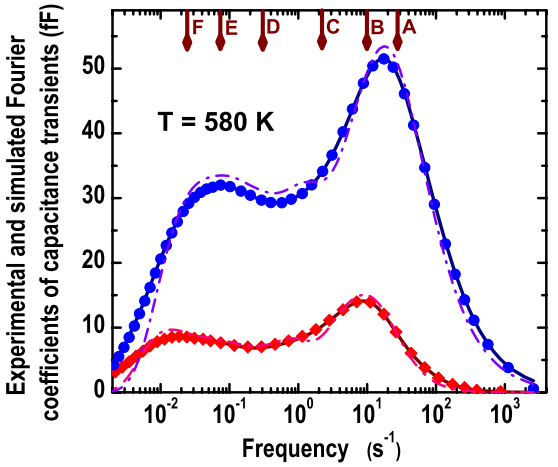

FIG. 7. (Color online) The imaginary and the real Fourier spectra of the capacitance transients at 580 K of boron-doped diamond (sample BM02): experimental data are shown, respectively, with circles and diamonds. The spectra calculated from the distribution function displayed in Fig. 6 are drawn in full lines and match exactly the previous ones. Spectra calculated from a multipeaked distribution function which retained only the contributions pertaining to the maxima of Fig. 6 are shown in dashed-dotted lines. The arrows associated to the letter i on the top of the figure refer to the frequency position of the H_{3i} trap.

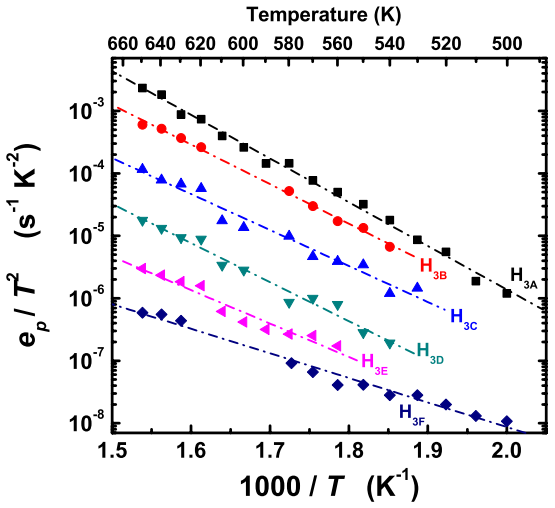

FIG. 8. (Color online) Arrhenius diagram, i.e., the hole emission rate divided by the square of the temperature (e_p/T^2) against $1000/T$ as defined in Eq. (1), deduced from the peak positions of the distribution functions of Fig. 6, plotted, respectively, with squares (H_{3A}), circles (H_{3B}), upward triangles (H_{3C}), downward triangles (H_{3D}), left triangles (H_{3E}), and lozenges (H_{3F}) for boron-doped diamond (sample BM02).

From the previous analysis, peak positions appearing in Fig. 6 at each temperature are representative of the most intense emission rates existing in each distribution function with some additional broadening due to original noisy data. Then, monitoring peak position as a function of the temperature allows to plot Arrhenius diagrams in a reciprocal temperature range of at least 0.3 in $1000/T$ units, as done in Fig. 8.

Corresponding ionization energies and capture cross-sections derived from HR-ITS in sample BM02 are added in Table I with H_{3i} labels (i=A,B,C,D,E,F) while hole traps H_{1i} and H_{2i} have been deduced either from studies in other samples or BM02 during the first thermal cycle as discussed in the last section. Capture cross-sections are checked with the same method as in Sec. III A except that the calculated emission rates are compared to the peak position of the distribution function in Fig. 6.

IV. *AB INITIO* CALCULATIONS

In order to investigate the electronic properties of possible candidates for the observed traps in B-doped diamond, we performed *ab initio* calculations concerning: (i) segregation of boron atoms, (ii) hydrogen atoms trapped near to boron atoms, and (iii) hydrogen atoms trapped in diamond without boron atom.

For boron dimers (two boron impurities per cell) several relative positions are considered. Starting from first-nearest neighbor positions (NN), we computed up to eight-nearest neighbor positions (8NN). It is found that first-nearest neighbors are most stable. These results contradict the boron dimer case in silicon, where two substitutional boron atoms prefer configurations remote from each other because of tensile stress.[64] Our calculation is in good agreement with the recent theoretical calculations for boron dimers in diamond matrix, where first-nearest-neighbor configurations were found to be about 200 meV more stable compare to the second-nearest neighbor within a different localized basis LDA approach.[23,65] Using the marker method as described in a previous work,[42] the ionization energy of the acceptor level of the dimer has been calculated at E_v+1.214 eV, in good agreement with the previous calculated acceptor level at E_v +1−1.2 eV by others.[23,24] The donor level is found at E_c −4.9 eV. These DFT calculations revealed the boron dimer which yields deep acceptor (E_v+1.214 eV) compared to isolated boron impurity (E_v+0.37 eV) in diamond. The deeper acceptor involved by boron dimers can be understood by the shift of the original acceptor level as suggested in Ref. 24.

Ab initio calculations for H and H_2 have been performed. Three different sites have been calculated for H: bond centered (BC), hexagonal (Hex), and tetrahedral (T). The most stable structure (BC) and its geometry are in good agreement with other recent results where the atomic positions are also relaxed.[38,41,66–68] For H_2 we considered the following configurations: H_2^* (one H at BC, the other one at the antibonding position), H_{2BC} (same than H_2^* with puckered positions), H_2^{TH} (one H at tetrahedral site the other one at the neighboring Hex site), H_2^{TT} (2 H at neighboring T sites). H_2^* is the most stable configuration in agreement with literature.[69,70] The acceptors levels of H and H_2 were found, respectively, at E_v+3.07 eV and E_v+4.69 eV. The donor levels of H and H_2 were found, respectively, at E_c−3.26 eV and E_c −4.84 eV.

The BH and BH_2 complexes have been theoretically investigated in a previous work.[42] The most stable structure and the associated ionization energies have been given. The acceptors levels of BH and BH_2 complexes were found, respectively, at E_v+4.44 eV and E_v+1.14 eV. The donor levels of BH and BH_2 complexes were found, respectively, at E_c−4.84 eV and E_c−2.80 eV. These values are also in good agreement with preceding works.[40,41,58]

V. DISCUSSION

In order to determine the origin of the deep DLTS traps, two different and complementary methods are generally used: (i) comparison of the free energy and capture cross-section with the calculated electronic properties of defects or impurities (like *ab initio* calculations, for example) and (ii) special behavior of the trap with some changing parameters (annealing, profile depth, presence of the impurity or not during the growth, etc, …). Here, a discussion about the origin of the different traps observed in this work will be given. In order to propose some possible candidates for each DLTS traps, we must consider the nature of the level (donor or acceptor) and the calculated transition energy [for example, (0/+)] from the *ab initio* part with the measured cross-section and the ionization energy from the experimental part. However, it must be notice that we will focus here on the electronic properties calculated for a trap level but we do not consider the probability for them to exist or not. Specific calculations concerning the formation energy must be done in order to validate this proposition.

A. Donor levels

The capture cross-section with values lower than 10^{-14} cm^2 are related to repulsive or neutral centers (nonattractive) and so correspond to donor traps in *p*-type material (hole capture). This is the case of the traps H_{1C}, H_{3B}, H_{3C}, H_{3D}, H_{3E}, and H_{3F} found in the samples of this work and H_{2A} from Refs. 32 and 35. Donor level means a change in the charge state of the center resulting in the addition of one + charge when an hole is captured [as, for example, (0/+) or (+/++), etc, …]. So, the ionization energies measured in this work have to be compared with these transition energies from theoretical works. Possible candidates are B and H related centers or intrinsic defects as interstitial or vacancy.

B_2, H_2, and BH complex donor levels (0/+) calculated in this work or in Ref. 42 have been found close to E_c −4.8 eV, corresponding to $\simeq E_v+0.6$ eV. This is at the same ionization energy than the donor level of the vacancy.[43] The H_{3F} level ($E_v+0.78$ eV) measured by HR-ITS which has an extremely low capture cross-section $\simeq 10^{-22}$ cm^2 is in good agreement with all these levels.

Concerning the BH_2 complex, the expected donor level is too deep to be observable with DLTS [$E_v+2.75$ eV (Ref. 42) and $E_v+2.60$ eV with negative-*U* system[41]). The atomic structure of the BH_3 complex is not clearly identified up to now but could create a donor level at $E_v+0.20$ eV.[41] This energy level is not in the DLTS window. The BH_4 complex is calculated to be a deep donor at $E_v+1.80$. eV (Ref. 41) which is deeper than the trap measured in this work.

A good candidate for the H_{1C} ($E_v+0.99$ eV), H_{2A} ($E_v+1.15$ eV), and H_{3i} ($E_v+1.06$ eV to $E_v+1.39$ eV) traps is the B_SV complex which is calculated at $E_v+1.0$ eV from the valence band.[24] Other possible traps for these centers are B_SVH or B_SVH_2 which are calculated as donor levels close to the valence band. It must be noticed that the H_{2A} (Refs. 32 and 35) and H_{3i} trap density is decreasing from the surface to the bulk. In the case of H_{3i}, the trap depth profiles are changing after temperature cycling.[71] H and vacancy are in good agreement with such kind of properties since these defects are able to move in diamond for this temperature range.

B_SVH_4 is a deep donor and B_2H, B_2H_2, B_i, and B_SI are donor levels too far from the valence band[41] to be observed. A summary of the deep donor levels related to boron, hydrogen, or native defects in the diamond band gap calculated by *ab initio* method and tentative assignments to traps observed by DLTS is given in Table II.

B. Acceptor levels

Only two trap levels measured in this work (H_{1B} and H_{3A}) can be attributed to acceptor due to their cross-section. The H_{1B} has a huge cross-section value of 1×10^{-11}–2×10^{-11} cm^2 and the H_{3A} at the limit of the neutral center. The H_{1A} trap observed in Refs. 32 and 35 has exactly the same free energy that H_{1B} but has a slightly smaller cross-section (2×10^{-12}–8×10^{-12} cm^2). As for donor levels, most of the defects are clearly not in the good energy range (B_3V, B_4V, B_2H, B_2, B_i, B_SI, B_SVH, BVH_2, BVH_3, and BVH_4).[41] Possible candidates for these three traps are the B dimers ($E_v+1.214$ eV) calculated in this work, the BH_2 ($E_v+1.14$ eV),[42] the B_2V ($E_v+1.6$ eV),[24] the B_SV ($E_v+1.9$ eV),[24] the divacancy ($E_v+1.7$ eV), and vacancy disk.[43] Starting from the hypothesis that $E_c-1.84$–2.88 and H_{1B} have the same origin but with different diameters (involving different cross-sections) of the attractive potential well (near 20 nm), the best candidate is the vacancy disk which is able to move for this temperature range as observed in Refs. 35 and 71.

A summary of the deep acceptor levels related to boron, hydrogen, or native defects in the diamond band gap calculated by *ab initio* method and tentative of attribution to traps observed by deep-level transient spectroscopy is given in Table III.

VI. CONCLUSION

Deep hole traps in boron-doped diamond have been investigated experimentally (deep-level transient spectroscopy and high-resolution isothermal spectroscopy) and theoretically (*ab initio* calculations). Nine different hole traps have been identified between 0.78 and 1.57 eV from the valence band. Comparing with calculations, some tentative assignments of the deep traps with donor or acceptor levels of native defects and/or hydrogen and/or boron complexes have been proposed.

ACKNOWLEDGMENTS

We gratefully acknowledge Pierre Nicolas Volpe (Institut Neel, Grenoble, France), J. Chevallier (GEMaC, Meudon, France), J. Barjon (GEMaC, Meudon, France), and R. Jones (University of Exeter, United Kingdom) for fruitful discussions. We are thankful to Agence Nationale pour la Recherche (ANR Programs No. 06 BLAN 0339-02 and No. ANR-BLAN-06-2-134411), France for providing financial support. We thank our technical staff (Bruno Fernandez and Khaled Ayadi) of Nanofab (Institut Neel, Grenoble, France).

*pierre.muret@grenoble.cnrs.fr
†julien.pernot@grenoble.cnrs.fr

[1] A. M. Edmonds, M. E. Newton, P. M. Martineau, D. J. Twitchen, and S. D. Williams, Phys. Rev. B **77**, 245205 (2008).
[2] G. Davies, S. C. Lawson, A. T. Collins, A. Mainwood, and S. J. Sharp, Phys. Rev. B **46**, 13157 (1992).
[3] J. A. Garrido, C. E. Nebel, M. Stutzmann, E. Gheeraert, N. Casanova, and E. Bustarret, Phys. Rev. B **65**, 165409 (2002).
[4] J. A. Garrido, C. E. Nebel, M. Stutzmann, E. Gheeraer, N. Casanova, E. Bustarret, and A. Deneuville, Diamond Relat. Mater. **11**, 347 (2002).
[5] A. Pu, V. Avalos, and S. Dannefaer, Diamond Relat. Mater. **10**,

585 (2001).
[6] P. Muret, C. Saby, F. Pruvost, and A. Deneuville, Diamond Relat. Mater. **9**, 1041 (2000).
[7] C. E. Nebel, R. Zeisel, and M. Stutzmann, Phys. Status Solidi A **174**, 117 (1999).
[8] R. Zeisel, C. E. Nebel, M. Stutzmann, E. Gheeraert, and A. Deneuville, Phys. Rev. B **60**, 2476 (1999).
[9] S. Koizumi, K. Watanabe, M. Hasegawa, and H. Kanda, Science **292**, 1899 (2001).
[10] J. A. Garrido, C. E. Nebel, R. Todt, G. Rösel, M.-C. Amann, M. Stutzmann, E. Snidero, and P. Bergonzo, Appl. Phys. Lett. **82**, 988 (2003).
[11] M. W. Geis, J. C. Twichell, J. Macaulay, and K. Okano, Appl. Phys. Lett. **67**, 1328 (1995).
[12] J. Pernot and S. Koizumi, Appl. Phys. Lett. **93**, 052105 (2008); J. Pernot, C. Tavares, E. Gheeraert, E. Bustarret, M. Katagiri, and S. Koizumi, *ibid.* **89**, 122111 (2006).
[13] P. N. Volpe, J. Pernot, P. Muret, and F. Omnès, Appl. Phys. Lett. **94**, 092102 (2009).
[14] J. Pernot, P. N. Volpe, F. Omnès, P. Muret, V. Mortet, K. Haenen, and T. Teraji, Phys. Rev. B **81**, 205203 (2010).
[15] M. I. Landstrass, M. A. Plano, M. A. Moreno, S. McWilliams, L. S. Pan, D. R. Kania, and S. Han, Diamond Relat. Mater. **2**, 1033 (1993).
[16] A. T. Collins, in *Properties and Growth of Diamond*, edited by G. Davies (INSPEC, London, 1994), Chap. 9.7, p. 288 and references therein.
[17] T. Klein, P. Achatz, J. Kačmarčik, C. Marcenat, F. Gustafsson, J. Marcus, E. Bustarret, J. Pernot, F. Omnes, B. E. Sernelius, C. Persson, A. Ferreira da Silva, and C. Cytermann, Phys. Rev. B **75**, 165313 (2007).
[18] E. Bustarret, J. Kačmarčik, C. Marcenat, E. Gheeraert, C. Cytermann, J. Marcus, and T. Klein, Phys. Rev. Lett. **93**, 237005 (2004).
[19] Y.-H. Chen, C.-T. Hu, and I.-N. Lin, Appl. Phys. Lett. **75**, 2857 (1999).
[20] Z. Teukam, J. Chevallier, C. Saguy, R. Kalish, D. Ballutaud, M. Barb, F. Jomard, A. Tromson-Carli, C. Cytermann, J. E. Butler, M. Bernard, C. Baron, and A. Deneuville, Nature Mater. **2**, 482 (2003).
[21] J. Barjon, J. Chevallier, F. Jomard, C. Baron, and A. Deneuville, Appl. Phys. Lett. **89**, 232111 (2006).
[22] J. Barjon, A. Mehdaoui, F. Jomard, J. Chevallier, C. Mer, M. Nesladek, P. Bergonzo, J. Pernot, F. Omnès, and A. Deneuville, Appl. Phys. Lett. **93**, 062108 (2008).
[23] J. P. Goss, P. R. Briddon, R. Jones, Z. Teukam, D. Ballutaud, F. Jomard, J. Chevallier, M. Bernard, and A. Deneuville, Phys. Rev. B **68**, 235209 (2003).
[24] J. P. Goss and P. R. Briddon, Phys. Rev. B **73**, 085204 (2006).
[25] D. C. Look, *Electronic Properties of GaAs Materials and Devices* (Wiley, New York, 1989).
[26] P. Blood and J. W. Orton, *The Electrical Characterization of Semiconductors: Majority Carriers and Electrons States* (Academic, San Diego, 1992).
[27] I. Thurzo, D. R. T. Zahn, and A. K. Dua, Semicond. Sci. Technol. **16**, 527 (2001).
[28] O. Gaudin, D. K. Troupis, R. B. Jackman, C. E. Nebel, S. Koizumi, and E. Gheeraert, J. Appl. Phys. **94**, 5832 (2003).
[29] K. Liu, C. Johnston, J. H. Chu, S. Roth, B. Zhang, and M. Wan, J. Appl. Phys. **82**, 286 (1997).
[30] H. Kiyota, H. Okushi, K. Okano, Y. Akiba, T. Kurosu, and M. Iida, Appl. Phys. Lett. **61**, 1808 (1992).
[31] M. Bruzzi, D. Menichelli, S. Pirollo, and S. Sciortino, Diamond Relat. Mater. **9**, 1081 (2000).
[32] P. Muret, J. Pernot, T. Teraji, and T. Ito, Appl. Phys. Express **1**, 035003 (2008).
[33] R. Zeisel, C. E. Nebel, and M. Stutzmann, J. Appl. Phys. **84**, 6105 (1998).
[34] C. Tavares, P. Muret, S. Koizumi, and F. Jomard, Phys. Status Solidi A **204**, 2985 (2007).
[35] P. Muret, J. Pernot, T. Teraji, and T. Ito, Phys. Status Solidi A **205**, 2179 (2008).
[36] J. Shim, E. K. Lee, Y. J. Lee, and R. M. Nieminen, Phys. Rev. B **71**, 035206 (2005).
[37] J. P. Goss, P. R. Briddon, R. Jones, and S. Sque, Diamond Relat. Mater. **13**, 684 (2004).
[38] J. P. Goss, R. Jones, M. I. Heggie, C. P. Ewels, P. R. Briddon, and S. Öberg, Phys. Rev. B **65**, 115207 (2002).
[39] Y. Yan, J. Li, S.-H. Wei, and M. M. Al-Jassim, Phys. Rev. Lett. **98**, 135506 (2007).
[40] E. B. Lombardi, A. Mainwood, and K. Osuch, Phys. Rev. B **70**, 205201 (2004).
[41] J. P. Goss, P. R. Briddon, S. J. Sque, and R. Jones, Phys. Rev. B **69**, 165215 (2004).
[42] A. Kumar, J. Pernot, A. Deneuville, and L. Magaud, Phys. Rev. B **78**, 235114 (2008).
[43] R. Jones, Diamond Relat. Mater. **18**, 820 (2009).
[44] M. Suzuki, H. Yoshida, N. Sakuma, T. Ono, and T. Sakai, Appl. Phys. Lett. **84**, 2349 (2004).
[45] http://www.phystech.de/products/dlts/dlts.htm
[46] S. Weiss and R. Kassing, Solid-State Electron. **31**, 1733 (1988).
[47] C. Eiche, D. Maier, M. Schneider, D. Sinerius, J. Weese, K. W. Benz, and J. Honerkamp, J. Phys.: Condens. Matter **4**, 6131 (1992).
[48] D. Maier, P. Hug, M. Fiederle, C. Eiche, D. Ebling, and J. Weese, J. Appl. Phys. **77**, 3851 (1995).
[49] G. Kresse and J. Hafner, Phys. Rev. B **47**, 558 (1993).
[50] J. P. Perdew and Y. Wang, Phys. Rev. B **33**, 8800 (1986).
[51] G. Kresse and J. Hafner, J. Phys.: Condens. Matter **6**, 8245 (1994).
[52] H. J. Monkhorst and J. D. Pack, Phys. Rev. B **13**, 5188 (1976).
[53] S. J. Sque, R. Jones, J. P. Goss, and P. R. Briddon, Phys. Rev. Lett. **92**, 017402 (2004).
[54] The underestimation of the gap width with DFT is a well-known problem of this approach.
[55] J. E. Northrup and S. B. Zhang, Phys. Rev. B **47**, 6791 (1993).
[56] J. P. Goss, M. J. Shaw, and P. R. Briddon, Top. Appl. Phys. **104**, 69 (2007).
[57] J. Coutinho, V. J. B. Torres, R. Jones, and P. R. Briddon, Phys. Rev. B **67**, 035205 (2003).
[58] S. J. Sque, Ph.D. thesis, University of Exeter, 2005.
[59] G. Makov and M. C. Payne, Phys. Rev. B **51**, 4014 (1995).
[60] L. Dobaczewski, P. Kaczor, I. D. Hawkins, and A. R. Peaker, J. Appl. Phys. **76**, 194 (1994).
[61] L. Dobaczewski, A. R. Peaker, and K. Bonde Nielsen, J. Appl. Phys. **96**, 4689 (2004).
[62] S. W. Provencher, Comput. Phys. Commun. **27**, 213 (1982).
[63] J. Weese, Comput. Phys. Commun. **69**, 99 (1992).
[64] N. Jun Yamauchi, N. Aoki, and I. Mizushima, Phys. Rev. B **63**, 073202 (2001).

[65] E. Bourgeois, E. Bustarret, P. Achatz, F. Omnès, and X. Blase, Phys. Rev. B **74**, 094509 (2006).
[66] J. P. Goss, J. Phys.: Condens. Matter **15**, R551 (2003).
[67] C. P. Herrero, R. Ramírez, and E. R. Hernández, Phys. Rev. B **73**, 245211 (2006).
[68] C. P. Herrero and R. Ramírez, Phys. Rev. Lett. **99**, 205504 (2007).
[69] A. B. Anderson, L. N. Kostadinov, and J. C. Angus, Phys. Rev. B **67**, 233402 (2003).
[70] S. P. Mehandru, A. B. Anderson, and J. C. Angus, J. Mater. Res. **7**, 689 (1992).
[71] P. Muret, A. Kumar, P.-N. Volpe, M. Wade, J. Pernot, L. Magaud, C. Mer, P. Bergonzo, Phys. Status Solidi A **206**, 2016 (2009).